

Supporting Information

Impregnation of paper with cellulose nanocrystal reinforced polyvinyl alcohol: synergistic effect of infrared drying and CNC content on crystallinity

*Johanna Desmaisons, Martine Rueff, Julien Bras, Alain Dufresne**

Univ. Grenoble Alpes, CNRS, Grenoble INP, LGP2, F-38000 Grenoble, France

Corresponding Author

* Alain Dufresne, Email: alain.dufresne@pagora.grenoble-inp.fr

Supporting information 1: Paper structure and penetration of the composite during the impregnation process

Scanning Electron Microscopy. Scanning electron microscopy (SEM). Observations were performed with an environmental SEM (ESEM) (Quanta 200©, FEI, Japan) on paper cross-section and surface after gold sputter coating of 5 nm, with a tension of 10 keV, and a spot size of 3.5 nm, in EDT mode. The working distance was 10 mm. At least 10 images were recorded for each sample and the most representative were selected.

CNC grafting with a fluorescent agent. A commercial fluorescent agent (Tinopal CBS, BASF, Germany) was used. This fluorescent agent consists of a 27 wt% solution of 4,4'-distyrybiphenyl sodium sulfonate salt (DSPB) with a molecular weight of 562 g.mol⁻¹. For the preparation of 15 g CNC (dry content), a dilute solution of DSPB was prepared by adding 0.250 g of pure solution to 45 g of water. Then, 0.5 g of the diluted solution was added to the 0.5 wt% CNC suspension and stirred for 15 min in a flask wrapped with aluminum foil to prevent photolysis of DSPB. The CNC was dialyzed against distilled water for at least one week, until no more fluorescence was detected in the washing water.

Optical microscopy of cross-sections with paper inclusion. Inclusion resin was prepared from a mixture of dibutyl phthalate and epichlorohydrin, called "Araldite M". An 11 g quantity of araldite was mixed with 12 g of dodeceny succinic anhydride (DDSA) and 0.6 g of benzyl dimethyl amine (BDMA). After stirring, the resin was degassed under vacuum for 2 h. The resin was then poured into individual molds 0.7 cm × 1.5 cm containing paper samples. The resin was then again degassed under vacuum for 5 h. Finally, polymerization of the resin was performed in an oven at 60 °C for 48 h. Tough resin blocks with embedded paper were recovered. A microtome was used to cut paper slices 7 μm thick. These slices were observed

with an optical microscope (Zeiss Axio Vert.A1, Germany). DSPB (fluorescent agent) absorbs in the UV spectral range (absorption wavelength 351 nm) and emits strong blue fluorescence (emission wavelength 425 nm). The reflector was chosen for an excitation wavelength ranging between 325 and 375 nm. Images were analyzed using AxioVision Release 4.8 and ImageJ software.

Zero-span Breaking length L_{r0} (km). The breaking length of paper was measured using a joined-clamp tensile device (Pulmac TS-100, USA) following the ISO:15361 method. Samples had a width of 15 mm and a length of 5 cm. All samples were stored in a conditioned room (23 °C, 50% RH) for at least 48 h before testing and 10 duplicates were performed to obtain average values. Wet samples were immersed for 1 min in water and pressed between two blotter papers to remove the excess water. The breaking length L_{r0} (km) was calculated using the following equation (1):

$$L_{r0} = \frac{F}{l \cdot g \cdot BW} \quad (1)$$

where F is the force at break (kgf), l is the sample width (0.015 m), g is the gravitational constant (9.8 m.s⁻²) and BW is the basis weight (g.m⁻²).

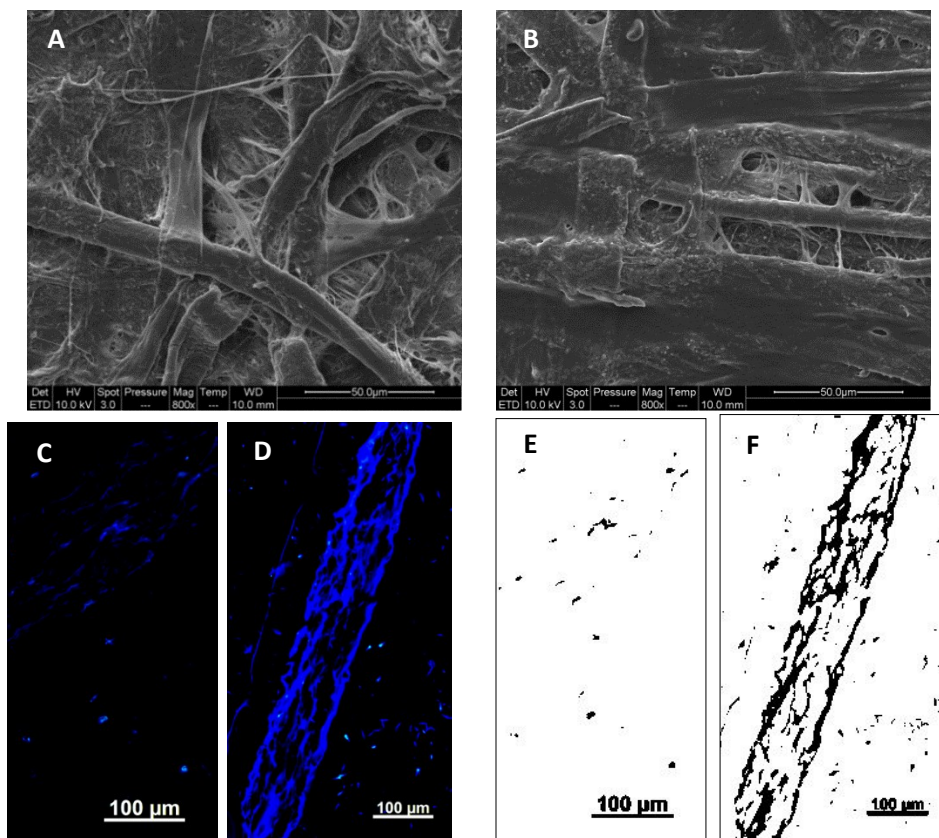
Results.

Paper was impregnated with neat PVOH or 10 wt% CNC-reinforced PVOH composite. SEM images of paper cross-sections before and after impregnation were not accurate enough to detect the presence of CNCs and consequently do not provide clues about their location. However, observation of the surface shows coverage of the fibers after impregnation with either neat PVOH or 10 wt% CNC-reinforced PVOH (Figures S1A and S1B, respectively). Thickness measurement of the paper impregnated with neat PVOH or 10 wt% CNC-reinforced PVOH shows an experimental value of $3.4 \pm 0.4 \mu\text{m}$ for the layer thickness, which

is 2 μm below the theoretical value obtained by calculation from basis weight (BW) and layer

density (ρ) (thickness = $\frac{BW}{\rho}$). As this difference is not due to paper swelling (since the same values were obtained for theoretical and experimental thickness for a paper impregnated with water), it could be due to penetration of the coating. Furthermore, we can still distinguish the fiber surface once it is impregnated, meaning that the multilayer organization as reported for plastic films cannot be considered.

To confirm this result, penetration of CNCs was followed by grafting a fluorescent agent to the surface of the nanoparticles. After impregnation and paper inclusion, observations with polarized optical microscopy show fluorescence not only at the surface but deep inside the material (Figures S1C and S1D). To better visualize the fluorescent agent, image with inverted colors are presented in Figures S1E and S1F.



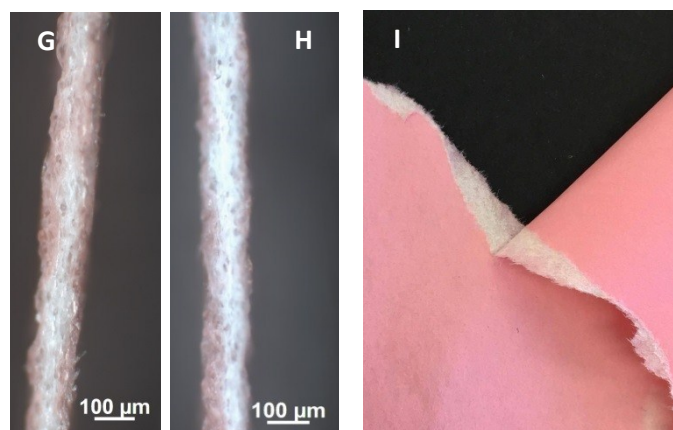


Figure S1. SEM images of the paper surface: (A) uncoated paper and (B) paper impregnated with neat PVOH. Optical micrographs of paper inclusion impregnated with (C,E) neat PVOH and (D,F) 10 wt% fluorescent CNC reinforced PVOH (C and D corresponds to real colors, and E and F to inverted colors). Optical micrographs of paper impregnated with (G) neat PVOH and (H) 10 wt% fluorescent CNC reinforced PVOH with addition of a red water dye in the impregnation bath. (I) Torn paper impregnated with red colored water impregnation bath.

The water pathway in the paper sheet during the impregnation process was also followed using a red azoic dye soluble in water (Figures S1G and S1H). Using ImageJ software, the penetration of water in paper was determined when impregnating with water, or a solution of 5 wt% PVOH or 10 wt% CNC-reinforced PVOH. The following results are described as a function of the total thickness of the paper. The water penetration for paper impregnated with only water was $70\% \pm 2$. This is confirmed in Figure S1I which shows that no dye is present in the middle of the paper once torn, confirming the partial penetration of water with our process. The solution penetration when using neat PVOH was very similar with a value of $60\% \pm 3$. The slight difference might be due to the slight difference in viscosity between water and PVOH solution. In the case of impregnation with 10 wt% CNC-reinforced PVOH composite, the water penetration was exactly the same as for neat PVOH, which is consistent with the fact that the addition of CNCs does not change the viscosity of PVOH and therefore its penetration. These results rule out the possibility of the multilayer model and attest to

significant penetration into the material. Furthermore, it can be seen that the penetration is asymmetric: this can be due to the asymmetric structure of the paper and asymmetric drying performed in this case with infrared lamps.

Figure 2 (in the manuscript) summarizes the possible structure of the impregnated paper. One question is still pending: do we have any individual fiber coating? To know if the penetration also leads to fiber reinforcement, tensile tests with joined clamps were performed on the paper before and after impregnation with water, neat PVOH or CNC-reinforced PVOH, to determine the breaking length value L_{r0} . This test is characteristic of fiber strength, and the wet results are independent of the impacts of drying and of fiber interconnection. It appears in Figure S3 that similar results are obtained before and after paper impregnation with water, PVOH or CNC-PVOH composite. In other words, no fiber reinforcement appears with impregnation of neat PVOH or CNC-reinforced PVOH. Furthermore, SEM images of fibers at the breaking area show similar morphologies and do not show any appearance of a coating layer around the fiber. The model of fiber reinforcement can consequently be excluded. It should also be mentioned that other experiments were carried out to improve the visualization of the final material, such as X-ray nanotomography and cartography of chemical elements inside the material (X-ray microanalysis of grafted CNCs), and introduction of a micro-robot to measure the bending force of a single fiber inside the SEM device. However, these experiments did not lead to successful results and did not allow us to make any conclusions.

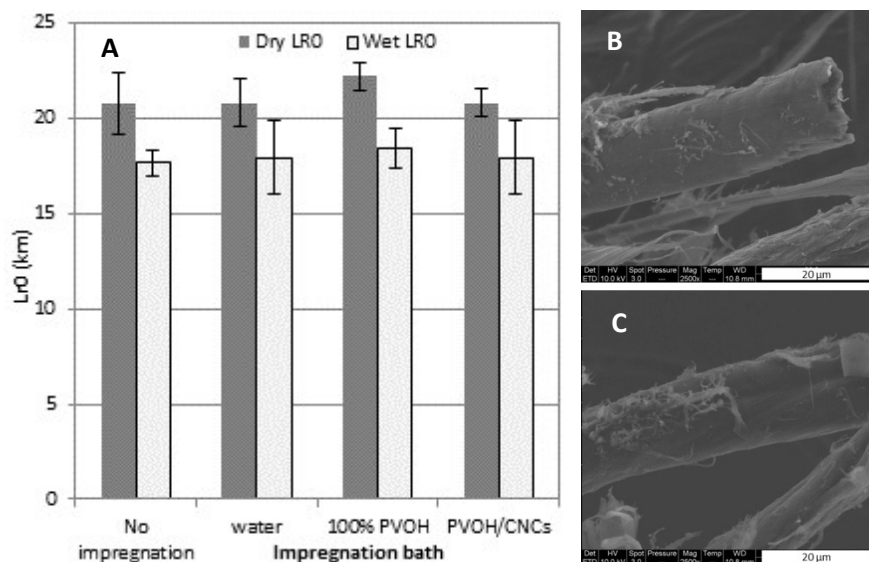


Figure S3. (A) Breaking length (Lr0/km) with joined clamps for dry samples and wet samples; SEM images of the fibers at the breaking point for (B) the uncoated paper and (C) the paper impregnated with 10 wt% CNC reinforced PVOH.

Supporting information 2: Long-wave infrared drying vs. convective drying temperature measurement

The heat transfer process differs between convective drying and radiative drying and this could affect the paper drying kinetics. Most of all, the energy inputs are not in the same range and are far higher for infrared. Moreover, the temperature of the paper surface significantly differs between these two drying conditions. Thermocouples were fixed on the paper surface to follow the paper temperature during classical convective drying of 3 min at 115 °C (Figure S4) and during 2 min infrared drying (Figure S5). The temperature of air inside the oven regulated at 115°C oscillates between 114 °C and 116 °C when the oven is empty. When the paper is drying, the air temperature at 10 cm from the paper surface averages 115 °C (Figure S4). However, the thermocouple fixed directly on the paper surface shows 4 different phases. First, there is a warm up period where the temperature of the test piece increases until a given temperature (here 47 °C). Secondly, the temperature remains constant and isothermal drying

takes place, during 100 s here. For convective drying (dispersion drying), a hot air flow is used to bring heat and remove water: heat is transferred to the product to evaporate liquid, and mass is transferred as a vapor into the surrounding gas. At the surface, a thin film of stagnant air is present. As evaporation is an endothermic phenomenon, the temperature at the paper surface is always lower than the temperature of the air and equilibrium is established between the rate of diffusion of water through the boundary layer and the heat transport of the air flow. During the third period, the temperature at the paper surface increases until reaching that of air (here 115 °C) at a rate of about 80 °C.min⁻¹. Once the paper is completely dried, its surface temperature is equal to that of the air. Consequently, during a 3 min drying process in an oven at 115 °C, the paper surface is actually at 115 °C for less than 40 s. It was found that this temperature evolution was exactly the same regardless of the impregnation bath formulation (neat PVOH or 10 wt% CNC reinforced PVOH).

In the case of infrared drying, the evolution of temperature at the paper surface is completely different: 200 °C is reached within only 10 s of drying and maintained during the whole drying process (Figure S5). Slight differences of a few degrees can be expected between the top and bottom surfaces, but this is accounted for because the thermocouple measuring the paper surface temperature at the top is in front of the incident light, and the value is consequently slightly over-estimated. We can thus only conclude that the real paper surface temperature at the top is between 180 °C and 200 °C, which is still a very high temperature. In this case, heat transfer takes place by coupling between the infrared radiation and OH groups from the water, and evaporation can be very fast. Such a difference in temperature at the surface of paper between convective and infrared drying has already been observed in previous studies for other applications^{1,2} and values obtained in this study agree with these previous observations.

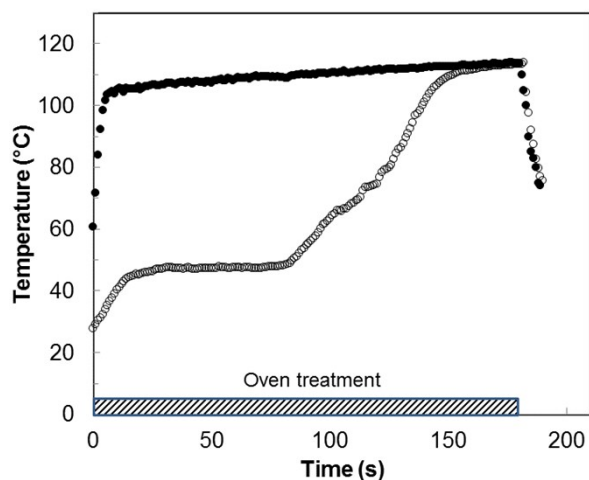


Figure S4. Evolution of the temperature in the oven (●) and at the surface of the paper (○) impregnated with neat PVOH, when applying 3 min convective drying (oven drying) at 115°C.

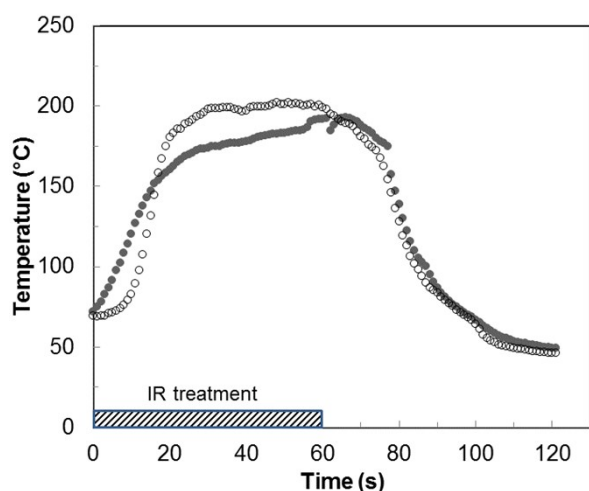


Figure S5. Evolution of the temperature at the surface of the paper (below (●) and above (○)) impregnated with neat PVOH, when applying 1 min long-wave IR drying (2500 W). This drying was carried out twice (1 min for each side of the paper).

References

- (1) Denneulin, A.; Blayo, A.; Neuman, C.; Bras, J. Infra-Red Assisted Sintering of Inkjet Printed Silver Tracks on Paper Substrates. *J. Nanoparticle Res.* **2011**, *13*, 3815-3823.

(2) Le Corre, D.; Bras, J.; Choisnard, L.; Dufresne, A. Optimization of the Batch Preparation of Starch Nanocrystals to Reach Daily Time scale. *Starch* **2012**, *64*, 489-496.